GEMINI NEAR-INFRARED SPECTROSCOPY OF LUMINOUS $z \sim 6$ QUASARS: CHEMICAL ABUNDANCES, BLACK HOLE MASSES, AND Mg II ABSORPTION[1]

Linhua Jiang[1], Xiaohui Fan[1], Marianne Vestergaard[1], Jaron D. Kurk[2], Fabian Walter[2], Brandon C. Kelly[1], and Michael A. Strauss[3]

ABSTRACT

We present Gemini near-infrared spectroscopic observations of six luminous quasars at $z = 5.8 \sim 6.3$. Five of them were observed using Gemini-South/GNIRS, which provides a simultaneous wavelength coverage of 0.9–2.5 μm in cross dispersion mode. The other source was observed in K band with Gemini-North/NIRI. We calculate line strengths for all detected emission lines and use their ratios to estimate gas metallicity in the broad-line regions of the quasars. The metallicity is found to be supersolar with a typical value of ~ 4 $Z_\odot$, and a comparison with low-redshift observations shows no strong evolution in metallicity up to $z \sim 6$. The Fe II/Mg II ratio of the quasars is 4.9 ± 1.4, consistent with low-redshift measurements. We estimate central BH masses of 10^9 to 10^{10} $M_\odot$ and Eddington luminosity ratios of order unity. We identify two Mg II $\lambda\lambda 2796,2803$ absorbers with rest equivalent width $W_0^{\lambda 2796} > 1$ Å at $2.2 < z < 3$ and three Mg II absorbers with $W_0^{\lambda 2796} > 1.5$ Å at $z > 3$ in the spectra, with the two most distant absorbers at $z = 4.8668$ and 4.8823, respectively. The redshift number densities (dN/dz) of Mg II absorbers with $W_0^{\lambda 2796} > 1.5$ Å are consistent with no cosmic evolution up to $z > 4$.

Subject headings: galaxies: high-redshift — galaxies: active — quasars: emission lines — quasars: absorption lines — quasars: general

[1]Steward Observatory, University of Arizona, 933 North Cherry Avenue, Tucson, AZ 85721

[2]Max-Planck-Institut für Astronomie, Königstuhl 17, D-69117 Heidelberg, Germany

[3]Department of Astrophysical Sciences, Princeton University, Princeton, NJ 08544

arXiv:0707.1663v1 [astro-ph] 11 Jul 2007

1. INTRODUCTION

In recent years we have witnessed the discoveries of quasars at $z \sim 6$; at this epoch the universe was less than one Gyr old (e.g. Fan et al. 2003, 2006; Cool et al. 2006; McGreer et al. 2006). These high-redshift quasars are among the most luminous objects known and provide direct probes of the early universe when the first generations of galaxies and quasars formed. Quasar activity and the formation processes of galaxies and supermassive black holes (BHs) are closely correlated (e.g. Kauffmann & Haehnelt 2000; Wyithe & Loeb 2003; Hopkins et al. 2005; Croton et al. 2006), so these $z \sim 6$ objects are essential for studying the accretion history of BHs, galaxy formation, and chemical evolution at very early epochs. High-redshift luminous quasars harbor BHs with masses of 10^9–10^{10} $M_\odot$ and emit near the Eddington limit (e.g. Barth et al. 2003; Vestergaard 2004; Jiang et al. 2006; Kurk et al. 2007), revealing the rapid growth of central BHs. Their emission line ratios show solar or supersolar metallicity, as is found in low-redshift quasars (e.g. Barth et al. 2003; Dietrich et al. 2003a; Freudling et al. 2003; Maiolino et al. 2003), indicating that there was vigorous star formation and element enrichment in the first Gigayear.

Understanding quasars requires observations from X-ray to radio wavelengths; each spectral region is due to different physical mechanisms and probes different regions of the active nucleus. In particular, the rest-frame UV spectrum, from the Lyα emission line to the Fe II bump at 2000–3000 Å, contains strong diagnostic emission lines and provides key information on the physical conditions and emission mechanisms of the broad-line region (BLR). The bulk motions of the BLR can be used to determine the mass of the central BH, while chemical abundances in the BLR are important in understanding the history of star formation in the host galaxy. Photoionization models show that various emission-line ratios provide reliable estimates of metallicity in the BLRs of quasars (e.g. Hamann et al. 2002; Nagao et al. 2006). Strong permitted line ratios, such as N V $\lambda 1240$/C IV $\lambda 1549$ (hereafter N V/C IV), N V $\lambda 1240$/He II $\lambda 1640$ (hereafter N V/He II), and Fe II/Mg II $\lambda 2800$ (hereafter Fe II/Mg II), are relatively easy to measure even in $z \sim 6$ quasars (e.g. Hamann & Ferland 1993, 1999). Fe abundance is of particular interest (e.g. Hamann & Ferland 1993, 1999): most of the Fe in the solar neighborhood is generated by Type Ia supernovae (SNe Ia), whose precursors are believed to be long-lived intermediate-mass stars in close binaries, so appreciable Fe enrichment can only happen on a timescale of one Gyr after the initial starburst (e.g. Greggio & Renzini 1983). On the contrary, the production of α elements such as Mg and O is dominated by SNe of types II, Ib and Ic, which explode very soon after the initial burst. Therefore, the Fe/α ratio is expected to be a strong function of age in young systems, and thus it puts a useful constraint on the age and chemical enrichment of the gas in the quasar environment.

At low redshift, elemental abundances measured from strong emission and intrinsic absorption lines have revealed that quasar environments have solar or supersolar metallicity. At $z \sim 6$, measurement of these spectral lines is difficult, as the rest-frame UV waveband is redshifted to the NIR range. NIR spectroscopy has been obtained for a few $z \sim 6$ quasars (e.g. Goodrich et al. 2001; Pentericci et al. 2002; Barth et al. 2003; Freudling et al. 2003; Maiolino et al. 2003; Stern et al. 2003; Iwamuro et al. 2004). These observations only provide NIR spectra with low signal-to-noise

ratios (SNRs) or partial wavelength coverage. Even basic properties such as the average continuum slope are not well measured. Recently, Kurk et al. (2007) obtained NIR spectra with high SNRs for a sample of five $z \sim 6$ quasars with ISAAC on VLT. They used the ISAAC data to study the Fe II/Mg II ratios, BH masses, and the Strömgren spheres around quasars. In this paper we present Gemini NIR spectroscopy of six $z \sim 6$ quasars. All these quasars were discovered by the Sloan Digital Sky Survey (SDSS; York et al. 2000) and were selected from Fan et al. 2000, 2001, and 2004 (hereafter quasar discovery papers). They have extensive follow-up observations in X-ray (e.g. Shemmer et al. 2006), *Spitzer* bands (e.g. Jiang et al. 2006), millimeter/submillimeter and radio wavelengths (e.g. Wang et al. 2007), providing a fundamental dataset to study luminous quasars at $z \sim 6$ in the context of the growth of early BHs and their relation to galaxy formation. The Gemini data have high SNRs and excellent NIR wavelength coverage. They are used to measure the metal abundances in high-redshift environments and estimate central BH masses using empirical mass scaling relations (e.g. McLure & Dunlop 2004; Vestergaard & Peterson 2006).

We also use these high-redshift spectra to study the evolution of strong intergalactic Mg II absorption at $z < 6$. Quasar absorption lines are an unbiased tracer of intervening gaseous material along the lines of sight to quasars. Strong Mg II absorption systems are usually directly associated with galaxy halos or disks (e.g. Charlton & Churchill 1998; Churchill et al. 2000; Steidel et al. 2002). The statistical properties of the Mg II $\lambda\lambda 2796,2803$ doublet absorbers at low redshift ($z \leq 2.2$) have been well studied (e.g. Steidel & Sargent 1992; Nestor et al. 2005; Prochter et al. 2006; see a summary of Mg II absorption surveys by Churchill et al. 2005). At higher redshift, the Mg II doublet is shifted to the NIR wavelength range, where detectors are much less efficient than are detectors at the optical region. The study of high-redshift Mg II absorbers is therefore limited by the small number of quasars with good NIR spectra available. Our Gemini/GNIRS spectra with high SNRs have excellent NIR wavelength coverage, so they are efficient to probe the Mg II absorption systems at $z < 6$.

The structure of the paper is as follows. In § 2 we describe our Gemini observations and data reduction of the six quasars. In § 3 we conduct a detailed spectral analysis, including the measurement of emission-line strengths. Chemical abundances are calculated and central BH masses are estimated in § 4. Mg II absorption systems in the quasar spectra are identified and analyzed in § 5. We give a brief summary in § 6. In this paper we use λ (λ_0) to denote observed-frame (rest-frame) wavelength. We use a Λ-dominated flat cosmology with $H_0 = 70$ km s^{-1} Mpc^{-1}, Ω_m = 0.3 and $\Omega_\Lambda = 0.7$ (Spergel et al. 2007).

2. OBSERVATIONS AND DATA REDUCTION

We obtained NIR spectra for the six luminous $z \sim 6$ quasars using Gemini-South/GNIRS and Gemini-North/NIRI. Five of them were chosen to be easily reached by Gemini-South, and were observed using GNIRS in February and March 2006. The observations on GNIRS were carried out in cross-dispersion mode, giving a simultaneous wavelength coverage of 0.9–2.5 μm with excellent

transmission. At $z \sim 6$, strong diagnostic emission lines such as C IV and Mg II are redshifted to this wavelength range, so GNIRS provides us an efficient way to collect NIR information for high-redshift quasars. We used the short camera on GNIRS with a pixel scale of $0.15''$/pixel. The slit length in cross-dispersion mode is $6.1''$ and we used a slit width of $0.675''$ to optimize the combination of resolution and light gain. The resolving power is about 800 and the dispersion varies from ~ 3 Å per pixel at 0.9 μm to ~ 6 Å per pixel at 2.5 μm. This is sufficient to separate the Mg II $\lambda\lambda 2796,2803$ doublet absorption lines. We used the standard ABBA nodding sequence between exposures. The exposure time at each nod position was five minutes and the distance between the two positions was $3''$. Before or after the exposure of each quasar, a nearby A or F spectroscopic standard star was observed for flux calibration and to remove telluric atmosphere absorption. The log of observations is given in Table 1, where redshifts, z_{AB} (AB magnitudes) and J (Vega-based magnitudes) are taken from the quasar discovery papers.

The GNIRS data were reduced using the Gemini package within IRAF[2]. Briefly, for each quasar the NIR spectroscopic data were sky-subtracted for each pair of images taken at the two nod positions. Then the images were flat-fielded. In cross-dispersion mode, GNIRS uses orders 3–8 to cover 0.9–2.5 μm. A single flat has non-uniform illumination between orders, so three sets of flats with different exposure times were taken each night. The final flat is extracted from the three flats so that each order has good illumination but without saturation. After flat-fielding, distortion correction and wavelength calibration were applied, the frames were combined, and one-dimensional spectra were extracted. Then the spectra were flux calibrated and corrected for telluric atmosphere absorption using the spectra of the spectroscopic standard stars. Finally the spectra in different orders were scaled and connected to a single spectrum. Adjacent orders cover a short common wavelength range, which enables the individual orders to be scaled to form a continuous, smoothly connected spectrum. This arbitrarily scaled spectrum was then calibrated to the J broad-band magnitude listed in Table 1 and thereby placed on an absolute flux scale with an uncertainty of 5$\sim$10%. The typical SNR at 1.2 μm reaches ~ 8 per pixel.

Figure 1 shows the spectra of the five quasars in the observed frame. The spectra at $\lambda \leq 1.0$ μm are taken from the quasar discovery papers. The spectra have been smoothed by three pixels. The bottom panel shows the sky transparency at an airmass of 1.0 and water vapor of 1.6 mm. There are strong telluric absorption bands around 1.4 and 1.9 μm, so we do not show the spectra in these ranges. In Figure 1 we also show a spectrum of a standard star HIP 54027 calibrated using the same procedure as we do for our science objects. For comparison, a spectrum (in red) of a black body with the effective temperature of HIP 54027 is given on top of the spectrum of HIP 54027. The good agreement between the two spectra indicate that spectra in different dispersion orders are properly scaled and connected.

We obtained a K-band spectrum for SDSS J1623+3112[3] using Gemini-North/NIRI in August and September 2004 and August 2005. The observations were made with a f/6 camera in spectroscopic mode. The long-slit has a length of $110''$ and we chose to use a slit width of $0.75''$, which provides a resolving power of ~ 500. The observing strategy and data reduction are similar to those used for the GNIRS data. The standard ABBA mode was used with a nodding distance of $20''$ and an exposure time of five minutes at each nod position. A nearby A or F spectroscopic standard star was observed before or after the target observation. The NIRI data were also reduced using the Gemini package within IRAF. After sky-subtraction, flat-fielding and wavelength calibration, the frames were combined. Then one-dimensional spectra were extracted from the combined images, and were flux calibrated using the spectra of standard stars. The observing log is given in Table 1 and the spectrum is shown in Figure 2. Since we do not have K-band photometry for this object, we cannot apply an absolute flux calibration. In Figure 2, we have scaled the spectrum to its J magnitude assuming a power-law continuum slope of $\alpha_\nu = -0.5$ ($f_\nu \sim \nu^{\alpha_\nu}$).

3.   SPECTRAL FIT AND EMISSION-LINE MEASUREMENTS

To analyze broad emission lines such as C IV and Mg II we fit and subtract the UV Fe II emission that contaminates most of the UV-optical spectral region; thousands of Fe II lines are emitted at UV-optical energies that blend with other lines in the spectrum. We use the UV Fe II template presented by Vestergaard & Wilkes (2001) and adopt the fitting procedure described in detail in § 4.2 by these authors. Briefly, the fitting is done as an iteration over a power-law fit to the continuum emission and a model fit to the Fe II emission using a scaled and broadened version of the Fe II template. The Fe II template is broadened by convolving the template with Gaussians with a range of sigmas. In the first iteration a power-law is fitted to regions with very little or no contribution from line emission (e.g. 1275–1295 Å; 1325–1335 Å; 1425–1480 Å; 2180–2220 Å; 3000–3040 Å). Upon subtraction of this primary continuum fit multiple broadened copies of the Fe II template are scaled to regions which predominantly contain Fe emission. The broadened, scaled Fe II template that provides the best overall match to the observed Fe II emission in the observed spectrum is then selected and subtracted. Some adjustments of the Fe II fitting regions are sometimes necessary to optimize the fit, as judged by a minimization of the residual flux upon subtraction of the Fe II model. After subtraction of the best matching Fe II model from the original data (i.e., with the continuum not subtracted) another power-law fit to the continuum emission is performed; the lack of (most of the) contaminating Fe II enables the fitting to be done over a broader wavelength range, often resulting in a better and more realistic continuum fit. After subtraction of this continuum model, the Fe II fitting is repeated. The iteration of the continuum and Fe II fitting is repeated until these individual fits do not change and the subtraction of the Fe II model

---

[3]The naming convention for SDSS sources is SDSS JHHMMSS.SS±DDMMSS.S, and the positions are expressed in J2000.0 coordinates as given in Table 1. We use SDSS JHHMM±DDMM for brevity.

leaves a smooth, featureless spectrum (barring the strong, broad non-Fe emission lines) with a realistic power-law slope. Convergence is often obtained in the second or third iteration. For SDSS J1623+3112, the wavelength range of the spectrum is too short to allow a reasonable fit to both the Fe II emission and a power-law continuum, so we assume a slope of $\alpha_\nu = -0.5$ during the model fitting. This gives a lower limit of the Fe II emission. Balmer continuum could be non-negligible at $\lambda_0 \geq 2000$ Å (e.g. Dietrich et al. 2002, 2003b), however, the wavelength coverage of our spectra is not long enough to provide a realistic fit to it, so we do not consider it in our fits. The power-law continuum fits to each of the quasars in our sample are listed in column 3 of Table 2. We note that the accuracy of the derived line width depends on the quality of the spectra. For widths broader than 5000–6000 km/s our ability to accurately determine the intrinsic Fe II line width decreases.

We use Mg II emission lines to determine the redshifts of the quasars. Accurate redshifts are important for various studies such as molecular line searches. The redshifts given in the quasar discovery papers were mostly determined from the Lyα emission lines, where strong Lyα absorption systems usually cause large uncertainties in redshift measurements. While most of high-ionization, broad emission lines such as C IV can be significantly blueshifted with respect to quasar systematic redshifts, the Mg II emission line has a small blueshift and thus provides a reliable redshift measurement (e.g. McIntosh et al. 1999; Vanden Berk et al. 2001; Richards et al. 2002). The Mg II emission line at $z \sim 6$ is close to a strong telluric absorption band at 1.9 μm, as seen in Figure 1. To avoid the effect of the telluric absorption, we measure the line center of each Mg II emission line using a Gaussian profile to fit the top $\sim 50\%$ of the line. The line center is also estimated by calculating the 3×median–2×mean mode of the top $\sim 50\%$ of the line. The two methods give similar results because the top $\sim 50\%$ of the line is almost symmetric. The measured redshifts are given in Column 2 of Table 2. They are in good agreement with the values derived in Kurk et al. (2007), but differ by 0.02–0.03 from the values in the discovery papers. We did not detect the Mg II emission line for SDSS J0836+0054 and SDSS J1044−0125, which were observed with high humidity. In Table 2, the redshift of SDSS J0836+0054, measured also using the Mg II emission line, is taken from Kurk et al. (2007), and the redshift of SDSS J1044−0125 is measured from the C III] λ1909 emission line using the same method.

We fit individual emission lines after the subtraction of the Fe II emission and power-law continuum. We use one Gaussian profile to fit most isolated lines and use multiple Gaussian profiles to fit blended lines. We allow both the line center and the line width to vary unless stated otherwise. Broad emission lines in quasars usually show asymmetric velocity profiles, so in the cases in which a single Gaussian profile does not provide a reasonable fit, we use double Gaussian profiles. There is no particular physical meaning to the two Gaussian components. For each quasar, the following emission lines (if detected) are fitted. (1) Lyα + N V + Si II λ1262 (hereafter Si II). We use four Gaussian profiles to fit the three lines, with the first two profiles representing the broad and narrow components of Lyα and the last two profiles representing N V and Si II, respectively. During the fit, the line centers are fixed at the values given by Vanden Berk et al. (2001). Since the blue side of the Lyα line is strongly absorbed, we only fit the red side of the Lyα line. (2) O I λ1304, C II λ1335, and

Si IV λ1397 (hereafter O I, C II, and Si IV). We use one Gaussian profile to fit each of these lines. (3) C IV. The strong C IV line is fitted using one or two Gaussian components. (4) He II + O III] λ1663 (hereafter O III]). These two lines are very weak, but He II is important for determining chemical abundances. They were tentatively detected in three quasars and fitted simultaneously using two Gaussians. (5) Al III λ1857 + C III] λ1909 (hereafter Al III and C III]). The weak Al III line is often detected on the blue wing of the strong C III] line. We use two Gaussian profiles to fit these two lines simultaneously if Al III is detected, otherwise the C III] line is fitted using a single Gaussian profile. We ignore the weak Si III] λ1892 line on top of C III]. (6) Mg II. The Mg II emission line can be well fitted by double Gaussians (e.g. Barth et al. 2003), with a weak component located on the blue side of a much stronger component. If the blue side of Mg II is affected by telluric absorptions, we fit the line using a single Gaussian. For the emission lines that are severely affected by broad-absorption lines (BALs), we fix their central wavelengths and fit their red half sides using a single Gaussian profile.

Figures 1 and 2 show the fitting results for the six quasars. The blue solid lines are the best fits to the emission lines and the blue dashed lines are the best model fits to the power-law continuum and Fe II emission. The red lines are the sums of all the components. For comparison, we show the low-redshift composite spectrum of Vanden Berk et al. (2001) in gray. Table 3 shows the rest-frame EW and FWHM of emission lines derived from the model fitting results. For the lines which were fitted using double Gaussian profiles, their EW and FWHM are calculated from the combination of the two components. The errors given in the table are the formal uncertainties obtained from our fitting process, so the real errors could be larger in the cases in which the lines are heavily blended, or we fit a profile of the wrong shape. The He II emission is tentatively detected in three quasars at a significance level of $\sim 2\sigma$. We note from Table 2 that three quasars have continuum slopes consistent with the slope $\alpha_\nu = -0.44$ of the composite spectrum of low-redshift SDSS quasars (Vanden Berk et al. 2001), while SDSS J1030+0524 and SDSS J1306+0356 show significantly bluer continua with $\alpha_\nu \sim 0.5$. Pentericci et al. (2003) obtained an average slope of $\alpha_\nu = -0.57$ with a scatter of 0.33 from 45 intermediate-redshift SDSS quasars at $3.6 < z < 5.0$. This indicates that the continuum slopes in the two unusual quasars deviate from the average slopes at a $\sim 3\sigma$ significance level. Table 2 also shows the rest-frame optical continuum slopes derived from the *Spitzer* IRAC broad-band photometry of the same objects (Jiang et al. 2006). The optical continua are generally redder than the UV continua measured from the Gemini spectra, as also reported by Vanden Berk et al. (2001).

4. CHEMICAL ABUNDANCES AND CENTRAL BH MASSES

4.1. Chemical Abundances

Emission-line ratios can be used to measure gas metallicity in the quasar BLR and track the chemical evolution with redshift. When weak emission lines are difficult to detect in high-

redshift quasars, strong broad emission lines such as N V, C IV, and Mg II become a powerful tool to probe metallicity at high redshift (e.g. Hamann & Ferland 1992, 1993). Different elements form on different timescales. Elements such as C, O, and Mg are formed in the explosions of massive stars, and their enrichment is rapid; while the second generation element N is produced from previously generated C and O, and its enrichment is relatively slow. Helium is a primordial element and its abundance changes little with cosmic time. Chemical abundances measured from emission lines and intrinsic absorption lines show solar or supersolar metallicity in quasar environments at low redshift (e.g. Hamann et al. 2007), and can be as high as 15 times solar metallicity (Baldwin et al. 2003). Furthermore, studies have shown that there is little chemical evolution up to the highest known redshift (e.g. Barth et al. 2003).

We calculate emission-line fluxes from the model fitting results described in § 3. The fluxes are normalized to the C IV fluxes and shown in Table 4 and Figure 3 (filled circles with errors). Nagao et al. (2006) used a sample of over 5000 quasars from the SDSS Data Release Two to study quasar BLRs. They made quasar composite spectra in the ranges of $2.0 \leq z \leq 4.5$ and $-29.5 \leq M_B \leq -24.5$, and measured emission-line ratios and metallicities in the composite spectra for each redshift and luminosity bin. They found that most of the line ratios (with respect to the C IV line) that they investigated do not show strong evolution with redshift. For the purpose of comparison, we show in Figure 3 the line ratios of quasars (filled squares) in the luminosity range of $-27.5 < M_B < -26.5$ from Nagao et al. (2006). Although there are correlations between quasar luminosities and most line ratios (Nagao et al. 2006), most of our quasars have luminosities in a small range of $-27.5 < M_B < -26.5$. Figure 3 shows that most of the flux ratios do not exhibit strong evolution up to $z \sim 6$. There is a trend for higher C II/C IV and O I/C IV ratios at higher redshift. Nagao et al. (2006) already noted that the O I/C IV flux ratio is marginally correlated with redshift. This trend could also be caused by the intrinsic dispersion of the flux ratios.

Photoionization models have shown that a series of emission-line ratios can be used to estimate gas metallicity in the BLRs of quasars. Hamann et al. (2002) studied the relative N abundance as a metallicity indicator based on the locally optimally emitting cloud (LOC) model (Baldwin et al. 1995), and calculated theoretical emission-line ratios as a function of metallicity $Z/Z_\odot$. We estimate the metallicity from the N V/C IV and N V/He II ratios using Figure 5 of Hamann et al. (2002). There is a 30% difference between the solar abundances used by Hamann et al. (2002) and the latest solar abundances (Baldwin et al. 2003), so we scale the abundances of Hamann et al. (2002) to match the latest values using the method by Baldwin et al. (2003). The results are shown as the open circles in Figure 4. Nagao et al. (2006) also used the LOC model, but included more UV emission lines in their photoionization model. We use Figure 29 of Nagao et al. (2006) to measure the metallicity from various line ratios and show the measurements as the filled circles in Figure 4. The two models give similar metallicities from the N V/C IV and N V/He II ratios. The metallicities in these high-redshift quasars are supersolar, with a typical value of $\sim 4 \, Z_\odot$. Nagao et al. (2006) computed chemical abundances as a function of redshift for the SDSS composite spectra using their photoionization model. The filled squares in Figure 4 show the abundances averaged in the

luminosity range of $-28.5 < M_B < -25.5$. The filled triangles represent the chemical abundances of eleven $3.9 < z < 5.0$ quasars from Dietrich et al. (2003a). Figure 4 shows that the metallicity is consistent with no strong evolution within the errors up to $z \sim 6$.

The Fe II/Mg II ratio is important in understanding chemical evolution at high redshift. We use the Fe II emission line complex at $\lambda_0 = 2000 \sim 3000$ Å as the Fe II flux indicator (e.g. Dietrich et al. 2002; Barth et al. 2003). The flux of the Fe II complex is integrated from 2200 to 3090 Å over the best-fitting Fe II template. The derived Fe II/Mg II ratios (filled circles) with a typical value of 4.9 ± 1.4 are shown in Table 4 and Figure 5. Using a similar method Kurk et al. (2007) obtained a lower ratio of 2.7 ± 0.8 from their quasar sample. The discrepancy is partly due to the fact that they corrected for Balmer continuum in their spectral fits. For comparison, we also show the Fe II/Mg II ratios of $z \sim 6$ quasars from previous measurements (Barth et al. 2003; Maiolino et al. 2003; Freudling et al. 2003; Iwamuro et al. 2004) as open circles in Figure 5. Iwamuro et al. (2002) measured the Fe II/Mg II ratios from the spectra of quasars at $0 < z < 5.3$, and computed the median values of the ratios for a range of redshifts. These median ratios are shown as the filled squares in Figure 5. To study the evolution of Fe II/Mg II, Dietrich et al. (2003b) made quasar composite spectra from $z = 0$ to 5. The Fe II/Mg II ratios measured from the composite spectra are shown as the filled triangles in Figure 5. We note that the Fe II flux in some studies was integrated over the wavelength range of $2150 < \lambda_0 < 3300$ Å (e.g. Freudling et al. 2003; Iwamuro et al. 2004), slightly different from the range that we used. We also note that some of these studies used different Fe II templates to measure Fe II fluxes. These issues usually affect the Fe II/Mg II measurements by less than a factor of two and cause a relatively large scatter in the measurements at $z \sim 6$. Figure 5 shows that our results are consistent with those derived from both low-redshift samples and other $z \sim 6$ samples within errors. Because the details of how the Fe II bump is formed are not well understood (e.g. Baldwin et al. 2004), so we do not derive actual abundances from the Fe II/Mg II ratios.

We have shown that the metallicity in the BLRs of high-redshift quasars is supersolar, and the lack of strong evolution in metallicity continues to $z \sim 6$. The high metallicity at $z \sim 6$ indicates that vigorous star formation and element enrichment have occurred in quasar host galaxies in the first Gyr of cosmic time. Millimeter and submillimeter observations revealed that luminous $z \sim 6$ quasars are extremely far-infrared (FIR) luminous ($\sim 10^{13}$ $L_\odot$) and have a large amount of cool dust (10^8–10^9 $M_\odot$) (Carilli et al. 2001; Bertoldi et al. 2003a; Priddey et al. 2003; Robson et al. 2004). If the FIR emission is mainly powered by star formation in host galaxies, the star formation rates are estimated to be ~ 1000 $M_\odot$ yr^{-1}. Strong starbursts can be induced by merging gas-rich galaxies (e.g. Hopkins et al. 2006; Li et al. 2007). CO observations have already revealed the presence of $\sim 2 \times 10^{10}$ $M_\odot$ of molecular gas in the highest redshift quasar SDSS J1148+5251 (Walter et al. 2003; Bertoldi et al. 2003b; Walter et al. 2004). This amount of gas can sustain the star formation rate of ~ 3000 $M_\odot$ yr^{-1}, inferred from the FIR luminosity, for 10^7–10^8 years. If the typical duty cycle time of luminous quasars is 10^7–10^8 years (e.g. Kauffmann & Haehnelt 2000; Wyithe & Loeb 2003; Shen et al. 2007), it would have enough time to form a large amount of first generation elements

from massive stars.

We have also shown that the Fe II/Mg II ratios of the $z \sim 6$ quasars are consistent with low-redshift measurements. Most of the Fe in the solar neighborhood is produced in intermediate-mass stars, and their enrichment is delayed by ~ 1 Gyr compared to Mg. Mg$^+$ and Fe$^+$ have similar ionization potentials and thus the Fe II/Mg II ratio reflects the Fe/Mg abundance (Dietrich et al. 2003b). Therefore, if Fe was generated in the same way as it is in our neighbors, the Fe II/Mg II ratio is expected to be a strong function of cosmic time at high redshift. However, we do not see any evolution in this ratio even at $z \sim 6$. It has been shown that the timescale of Fe enrichment from SNe Ia strongly depends on star formation histories of host galaxies, and can be much shorter in high-redshift quasar environments (e.g. Friaca & Terlevich 1998; Matteucci & Recchi 2001). Matteucci & Recchi (2001) found that the timescale for the maximum SN Ia rate (Fe enrichment) can be as short as ~ 0.3 Gyr in an elliptical galaxy with a high star formation rate but a short star formation history. On the other hand, Venkatesan et al. (2004) pointed out that stars with a present-day initial mass function are sufficient to produce the observed Fe II/Mg II ratios in $z \sim 6$ quasars, and SNe Ia are not necessarily the main contributor. Fe could also be generated in Population III stars, which are suggested to be first generation stars with masses between 100 and 1000 M$_\odot$. These very massive stars produce a large amount of Fe within a few Myr due to their short lifetimes (Heger & Woosley 2002).

4.2. Central BH Masses

The central BH masses of high-redshift quasars are important in understanding the growth of BHs and quasar accretion rates in the early universe. For high-redshift quasars where direct mass measurements are difficult, BH masses can be estimated using mass scaling relations based on broad emission line widths and continuum luminosities. Strong emission lines, including Hβ, C IV, and Mg II, have been used to determine BH masses (e.g. Wandel et al. 1999; Dietrich & Hamann 2004; McLure & Dunlop 2004; Vestergaard & Peterson 2006). Based on empirical scaling relations, a few luminous $z \sim 6$ quasars have been found to harbor central BHs with masses of $10^9 \sim 10^{10}$ M$_\odot$ (e.g. Barth et al. 2003; Vestergaard 2004).

We estimate the central BH masses for the six quasars using the following BH mass scaling relations,

$$M_{\rm BH}(\text{C IV}) = 4.57 \left(\frac{\text{FWHM}(\text{C IV})}{\text{km s}^{-1}} \right)^2 \left(\frac{\lambda L_\lambda(1350\text{Å})}{10^{44} \text{ ergs s}^{-1}} \right)^{0.53} M_\odot \tag{1}$$

and

$$M_{\rm BH}(\text{Mg II}) = 3.2 \left(\frac{\text{FWHM}(\text{Mg II})}{\text{km s}^{-1}} \right)^2 \left(\frac{\lambda L_\lambda(3000\text{Å})}{10^{44} \text{ ergs s}^{-1}} \right)^{0.62} M_\odot \tag{2}$$

derived by Vestergaard & Peterson (2006) and McLure & Dunlop (2004), respectively. L$_\lambda$(1350Å) and L$_\lambda$(3000Å) are luminosities at rest-frame 1350 and 3000 Å. The results are listed in Columns

4 and 5 of Table 5. They are in agreement with the masses derived by Kurk et al. (2007). For SDSS J1030+0524 and SDSS J1306+0356, the C IV–based BH masses are greater than the Mg II–based BH masses by a factor of $\sim$3, but still within the intrinsic scatter (a factor of 3–4) in these scaling relations. The unusual blue continua in the two quasars could cause this discrepancy. The Mg II–based BH masses are also estimated using the latest scaling relation based on FWHM(Mg II) and L$_\lambda$(1350Å) by Vestergaard et al. (in preparation). The results are shown in Column 6, and they are consistent with the C IV–based BH masses. Similar to other luminous quasars at $z \sim 6$, our quasars have central BH masses of 10^9–10^{10} M$_\odot$ (e.g. Barth et al. 2003; Vestergaard 2004; Jiang et al. 2006).

We calculate the Eddington luminosity ratios of the quasars using their bolometric luminosities and BH masses. We use the Mg II–based BH mass for SDSS J1623+3112 and the C IV–based BH masses for the others. The bolometric luminosities were calculated from multiband observations of the quasars by Jiang et al. (2006). The results are given in Column 3 of Table 5. These luminous $z \sim 6$ quasars have Eddington ratios of order unity, comparable to quasars with similar luminosities at lower redshift (e.g. McLure & Dunlop 2004; Vestergaard 2004; Kollmeier et al. 2006).

It is remarkable that billion-solar-mass BHs can form less than one Gyr after the Big Bang. With the reasonable assumption that BH accretion is at the Eddington rate, the BH mass at time t is $M_t = M_0 e^{t/\epsilon\tau}$, where ϵ is the radiative efficiency, $\tau = 4.5 \times 10^8$ years, and M_0 is the initial BH mass or the seed BH mass. Seed BHs can be produced from the collapse of Population III stars or gas clouds, and their masses are roughly 10^2–10^4 M$_\odot$ (e.g. Madau & Rees 2001; Volonteri & Rees 2006; Lodato & Natarajan 2007). Consider the case in which a massive BH at $z = 6$ formed from a seed BH with $M_0 = 10^3$ M$_\odot$ at $z = 20$. The e-folding time $\epsilon\tau$ for the BH growth is roughly 4.5×10^7 years if $\epsilon \sim 0.1$. The BH grows from $z = 20$ to 6 by 15 e-foldings, or a factor of 3.3×10^6, which results in a massive BH with $M_t = 3.3 \times 10^9$ M$_\odot$ at $z = 6$, comparable to the observed BH masses in our sample. If a quasar is shining at half of the Eddington limit, its BH grows from $z = 20$ to 6 by only 7.5 e-foldings, or a factor of ~ 2000, making it very difficult to form billion-solar-mass BHs in this scenario. In addition, if Eddington-limited accretion is via standard thin disks, BHs are likely to be spun up and the radiative efficiency and Eddington timescale will increase (Volonteri & Rees 2006; Rees & Volonteri 2006). In this case it would take much longer to form massive BHs. So super-Eddington accretion or lower radiative efficiency is probably required to form BHs with $M_t = 10^9$–10^{10} M$_\odot$ by $z = 6$.

4.3. Notes on Individual Objects

SDSS J0836+0054 ($z = 5.810$). SDSS J0836+0054 was discovered by Fan et al. (2001). Its redshift estimated from the Lyα emission line is 5.82, comparable to the redshift 5.810 ± 0.003 determined from the Mg II emission line (Kurk et al. 2007). Due to high humidity, we did not detect the Mg II emission line. Stern et al. (2003) found a very red continuum slope of $\alpha_\nu = -1.55$ in their NIR spectrum of this quasar. However, using the GNIRS spectra with a longer wavelength coverage

and a higher spectral quality we obtained a slope of $\alpha_\nu = -0.62$, which is close to $\alpha_\nu = -0.44$, the slope of the SDSS composite spectrum (Vanden Berk et al. 2001). SDSS J0836+0054 is the most luminous quasar known at $z > 5.7$. The central BH mass estimated from the C IV emission line is 9.5×10^9 M$_\odot$. It was also detected by the Faint Images of the Radio Sky at Twenty-cm (FIRST; Becker et al. 1995). The flux at 1.4 GHz measured by FIRST is 1.11±0.15 mJy and measured by Petric et al. (2003) is 1.75±0.04 mJy.

SDSS J1030+0524 ($z = 6.309$)**.** SDSS J1030+0524 is the second highest redshift quasar known to date. The redshift estimated from Lyα is 6.28 (Fan et al. 2001). We obtained a more accurate and slightly higher redshift 6.309 ± 0.009 from Mg II, consistent with the value 6.311 of Iwamuro et al. (2004). The emission-line ratios and metallicity in this object have been studied by a few groups. In the discovery paper Fan et al. (2001) estimated lower limits for the N V/C IV and N V/He II ratios: N V/C IV ≥ 0.4 and N V/He II ≥ 3.0. Using VLT NIR observations Pentericci et al. (2002) found N V/C IV $= 0.35$ and N V/He II > 4.3. From our measurements we obtained N V/C IV $= 0.21\pm0.02$ and N V/He II $= 2.85\pm1.70$, comparable to the previous studies. The Fe II/Mg II ratios of this object measured in previous papers are quite different. The values reported by Maiolino et al. (2003), Freudling et al. (2003), and Iwamuro et al. (2004) are 8.65 ± 2.47, 2.1 ± 1.1, and $0.99^{+1.86}_{-0.99}$, respectively. We obtained Fe II/Mg II $= 5.46 \pm 0.90$, consistent with the result of Maiolino et al. (2003). Note that the Fe II flux in Freudling et al. (2003) and Iwamuro et al. (2004) was integrated over the wavelength range $2150 < \lambda_0 < 3300$ Å, slightly different from the range $2200 < \lambda_0 < 3090$ Å that Maiolino et al. (2003) and we used. In addition, our NIR spectra have much higher SNRs than those of previous studies.

SDSS J1044−0125 ($z = 5.778$)**.** SDSS J1044−0125 was the first quasar discovered at $z > 5.7$ (Fan et al. 2000). The redshift estimated from Lyα is 5.80 (Fan et al. 2000) and that estimated from C IV is 5.74 (Goodrich et al. 2001). However, these measurements could be severely affected by absorption since this is a BAL quasar (Goodrich et al. 2001; Djorgovski et al. 2001). Due to high humidity we did not detect its Mg II emission line. The redshift measured from C III] (Figure 1 shows that this line is not affected by absorption) is 5.778 ± 0.005, consistent with the value 5.78 obtained by Freudling et al. (2003). Freudling et al. (2003) also reported a Fe II/Mg II ratio of 5.0 ± 2.1 for this quasar. SDSS J1044−0125 has the highest BH mass of the objects in our sample. Submillimeter observations (Priddey et al. 2003) and *Spitzer* observations (Jiang et al. 2006) revealed a large amount of cool and hot dust in this object. SDSS J1044−0125 is the only BAL quasar in our sample. The fraction of BAL quasars in the sample is 16.7%, similar to the low-redshift fraction (Trump et a. 2006).

SDSS J1306+0356 ($z = 6.016$)**.** The discovery paper for SDSS J1306+0356 indicated a redshift $z = 5.99$ based on Lyα (Fan et al. 2001). We obtained a more accurate and slightly higher redshift 6.016 ± 0.005. Pentericci et al. (2002) reported a N V/C IV ratio of 0.67 for this quasar. The ratio we measured is 0.55 ± 0.05. We also obtained a Fe II/Mg II ratio of 5.77 ± 0.72, slightly smaller than the value 9.03 ± 2.26 derived by Maiolino et al. (2003) based on low SNR spectra. We detected four strong Mg II $\lambda\lambda2796,2803$ absorption systems in the spectra of this quasar, including

the two highest redshift Mg II absorbers known (see § 5).

SDSS J1411+1217 ($z = 5.927$). SDSS J1411+1217 has the narrowest emission lines in our sample. Its Lyα and N V emission lines are well separated. Therefore the redshift $z = 5.93$ measured from N V and O I in the discovery paper (Fan et al. 2004) is accurate, and is consistent with the redshift 5.927 ± 0.004 measured from Mg II in the Gemini spectrum. SDSS J1411+1217 has the lowest BH mass in the sample. It also has a very weak *Spitzer* 24μm ($\lambda_0 \sim 3.5$ μm) flux, and its SED does not show any hot dust emission (Jiang et al. 2006). Another quasar SDSS J0005$-$0006 (not in this sample) shows similar IR properties and does not have hot dust emission either. This may reflect dust evolution at high redshift, as such dustless quasars are unknown at lower redshift.

SDSS J1623+3112 ($z = 6.247$). The redshift of SDSS J1623+3112 measured from Lyα in the discovery paper is 6.22. We obtained a higher redshift of 6.247 ± 0.005 from Mg II. This makes it the third highest redshift quasar known to date.

5. Mg II ABSORPTION SYSTEMS AT $z < 6$

We search for Mg II $\lambda\lambda 2796,2803$ intervening systems in the spectra of five $z \sim 6$ quasars. SDSS J1623+3112 is excluded in this analysis because it has a short wavelength coverage. The SNRs of the spectra for different quasars are different, as are the dispersions from one order to another. The SNRs at $\lambda \leq 1.2$ μm are usually higher than those at longer wavelengths, especially in the range of $1.4 < \lambda < 1.8$ μm (roughly H band). However, a Mg II $\lambda 2796$ absorption line with rest equivalent width $W_0^{\lambda 2796}$ greater than 1.0 Å at $z < 3$ or a Mg II $\lambda 2796$ absorption line with $W_0^{\lambda 2796}$ greater than 1.5 Å at $z > 3$ can be detected at a $\sim 7\sigma$ significance level in the lowest SNR parts of the spectra shown in Figure 1. Moreover, previous studies have used similar limits (e.g. Nestor et al. 2005). Our sample is small, and does not provide good statistics by itself, so the comparison with other samples is important. Thus to achieve unbiased statistics, we search for Mg II absorbers with $W_0^{\lambda 2796} > 1.0$ Å at $z < 3$ and Mg II absorbers with $W_0^{\lambda 2796} > 1.5$ Å at $z > 3$.

We search for pairs of absorption lines with separation matching the Mg II $\lambda\lambda 2796,2803$ doublet. Then we search for absorption lines of other species associated with the identified Mg II absorbers by matching various strong quasar absorption lines known in the literature to the spectra. Five Mg II absorption systems are identified, with one in the spectrum of SDSS J0836+0054 and the other four in the spectra of SDSS J1306+0356. We normalize the absorption lines using the local continua measured by fitting low-order spline curves to the spectra. Figure 6 shows the normalized spectra of the five absorption systems, with the identified lines marked. These lines are usually strong and commonly detected in quasar absorption systems, such as C IV $\lambda\lambda 1548,1550$ (marked as C IV-D in the figure), Fe II $\lambda 1608$, Al II $\lambda 1670$, Al III $\lambda\lambda 1854,1862$ (marked as Al III-D), Fe II $\lambda 2600$, Mg II $\lambda\lambda 2796,2803$ (marked as Mg II-D), and Mg I $\lambda 2852$. The four absorption systems found in the spectra of SDSS J1306+0356 are denoted as (a), (b), (c), and (d).

We measure the redshifts (z_{abs}) and rest-frame equivalent widths (W_0) of the absorption lines

by fitting a Gaussian to each line. Unresolved or very weak absorption lines are not fitted. The results are given in Table 6. The Mg II doublet ratios are close to one, indicating that these strong Mg II absorbers are saturated. The Mg II absorber identified in the spectra of SDSS J0836+0054 is at $z = 3.742$. A pair of moderate strong Al III $\lambda\lambda1854,1862$ lines in the same absorber are also detected. C IV $\lambda\lambda1548,1550$, which is usually associated with Mg II, is beyond the spectral coverage. We do not detect any strong Fe II absorption in this system. There are four Mg II absorption systems identified in the spectra of SDSS J1306+0356. Systems (a) and (b) are at relatively low redshifts. System (a) at $z = 2.202$ has a strong Mg I $\lambda2852$ absorption line. System (b) at $z = 2.532$ has a strong Fe II $\lambda2600$ absorption line. C IV $\lambda\lambda1548,1550$ in both systems is beyond the spectral coverage. We discovered two strong Mg II $\lambda\lambda2796,2803$ absorbers at $z = 4.8668$ and 4.8823. They are the most distant Mg II absorbers known to date. The Mg II $\lambda2803$ line in system (c) and the Mg II $\lambda2796$ line in system (d) almost exactly overlap with each other, so we do not calculate W_0 for the two lines. Note that this is not the so-called line-locking effect, which mainly occurs in BAL quasars or other associated absorption systems with $z_{abs} \sim z_{em}$ (e.g. Foltz et al. 1987; Vilkoviskij & Irwin 2001; Fechner et al. 2004), since the two absorbers are far from SDSS J1306+0356. The proper distance between the two absorbers is about 1.4 Mpc, so they are not likely associated with the same galaxy, but could still belong to the same large-scale structure. Both absorption systems have strong Al II $\lambda1670$ and Fe II $\lambda2600$ absorption and weak Fe II $\lambda1608$ and Al III $\lambda\lambda1854,1862$ absorptions. The C IV $\lambda\lambda1548,1550$ absorption is strong in system (c) but very weak in system (d). It has been found that C IV $\lambda\lambda1548,1550$ is almost always detected in strong Mg II absorption systems at low redshift (e.g. Steidel & Sargent 1992). The weakness of C IV in system (d) indicates that it is a rare, C IV-deficient system (Churchill et al. 2000). Elston et al. (1996) discovered a strong Mg II absorber at $z = 4.38$ in the spectrum of a $z = 4.68$ quasar. They found that the C IV absorption in this system is also very weak. Thus among the three strong Mg II absorbers at $z > 4$, two have very weak associated C IV, probably indicating that $z > 4$ absorption systems are in a lower ionization state than their low-redshift counterparts (Elston et al. 1996).

We calculate the comoving line-of-sight number densities (dN/dz) of the Mg II absorbers. The sample of the five Mg II absorbers is divided into two subsamples, one with $W_0^{\lambda2796} > 1$ Å at $z < 3$ and the other one with $W_0^{\lambda2796} > 1.5$ Å at $z > 3$. The redshift path covered by a spectrum is,

$$\Delta Z(W_0^{\lambda2796}) = \int_{\Delta z} g(W_0^{\lambda2796}, z)dz, \tag{3}$$

where $g(W_0^{\lambda2796}, z) = 1$ if a Mg II absorber at redshift z and of the given EW would be detected in the spectrum in the redshift range Δz and $g(W_0^{\lambda2796}, z) = 0$ otherwise. The total redshift paths covered by the two subsamples are 3.4 and 10.4, respectively. Then the number density along the redshift path for each subsample is estimated by,

$$dN/dz = \frac{N_a}{\sum \Delta Z(W_0^{\lambda2796})_i}, \tag{4}$$

where N_a is the number of Mg II absorbers and the sum is over all spectra in the subsample. We show our results in Figure 7. The filled diamond represents the density for $W_0^{\lambda2796} > 1.0$ Å at $z < 3$

and the filled circle represents the density for $W_0^{\lambda 2796} > 1.5$ Å at $z > 3$. The two data points are positioned at the median redshifts $z = 2.6$ and 4.3, respectively. The statistical uncertainties are Poisson.

The number density of Mg II absorbers at low redshift has been well studied. Steidel & Sargent (1992) collected the spectra of 103 quasars and found that the density of Mg II absorbers with $W_0^{\lambda 2796} > 0.3$ Å does not shows cosmic evolution, but the density of strongest Mg II absorbers significantly increases with redshift. Nestor et al. (2005) reached similar results by studying Mg II absorptions in the spectra of thousands of quasars from the SDSS Early Data Release (Stoughton et al. 2002). They divided the sample into subsamples with $W_0^{\lambda 2796} > 0.3$, 0.6, 1.0, 1.5, 2.0, 2.5, and 3.0 Å, respectively, and concluded that dN/dz of the $W_0^{\lambda 2796} > 0.3$, 0.6, 1.0, and 1.5 Å subsamples are consistent with no evolution within errors, while the densities of the other three subsamples show strong evolution with redshift. For comparison, we show in Figure 7 the $W_0^{\lambda 2796} > 1.0$ and 1.5 Å samples (open diamonds and circles) of Nestor et al. (2005). Prochter et al. (2006) studied strong Mg II absorption systems using an even larger quasar sample from the SDSS Data Release Three (Abazajian et al. 2004). They found that there is no evolution in the densities of $W_0^{\lambda 2796} > 1.0$ Å absorbers at $0.8 < z < 2.0$. The crosses in Figure 7 show the densities for their $W_0^{\lambda 2796} > 1.0$ Å sample (they did not use a sample of $W_0^{\lambda 2796} > 1.5$ Å). In Figure 7 we also show the non-evolution curves (dashed lines) for the cosmology of $(\Omega_m, \Omega_\Lambda, h) = (0.3, 0.7, 0.7)$ with zero curvature,

$$dN/dz = N_0(1 + z)^2[\Omega_m(1 + z)^3 + \Omega_\Lambda]^{-1/2}, \tag{5}$$

where N_0 is a normalization constant. The curves have been scaled to minimize the χ^2 to the data of Nestor et al. (2005). The density of Mg II absorbers with $W_0^{\lambda 2796} > 1.5$ Å that we have measured is consistent with no cosmic evolution up to $z > 4$. However, due to the large uncertainty, we cannot rule out the density evolution of Mg II absorbers.

6. SUMMARY

We have obtained high-quality NIR spectra of six luminous $z \sim 6$ SDSS quasars from our Gemini observations. Five of them were observed using Gemini-South/GNIRS in cross dispersion mode, which provides a simultaneous coverage of 0.9–2.5 μm. The sixth was observed in K band with Gemini-North/NIRI. These spectra have higher SNRs and better wavelength coverage than those in previous studies. We use the NIR spectra combined with optical data to study chemical abundances and BH masses in the $z \sim 6$ quasars and strong intergalactic Mg II absorption at $2.2 < z < 6$.

The spectra are fitted using a combination of a power-law continuum, an Fe II emission template, and a series of emission lines. We calculate the fluxes for detected emission lines based on the Gaussian model fitting results. We find that the line flux ratios (normalized to the C IV fluxes) that we have investigated do not show strong evolution with redshift. We calculate gas metallicity from emission-line ratios using the results of photoionization models given by previous studies and

find that the metallicity in the BLRs of these high-redshift quasars is supersolar with a typical value of ~ 4 $Z_\odot$. The comparison with low-redshift observations shows no show strong evolution in metallicity up to $z \sim 6$. The Fe II/Mg II ratio is also measured for each quasar. We find a typical Fe II/Mg II ratio of 4.9 ± 1.4, which is consistent with low-redshift samples. All these measurement indicate the existence of vigorous star formation and element enrichment in host galaxies in the first Gyr after the Big Bang. We have estimated central BH masses from the C IV and Mg II emission lines using empirical mass scaling relations. As found in other luminous $z \sim 6$ quasars, these quasars have BH masses of 10^9–10^{10} $M_\odot$ and Eddington luminosity ratios of order unity.

We have searched for strong Mg II $\lambda\lambda2796,2803$ intervening systems in the spectra of five quasars. Two Mg II absorbers with rest equivalent width $W_0^{\lambda2796} > 1$ Å at $2.2 < z < 3$ and three absorbers with $W_0^{\lambda2796} > 1.5$ Å at $z > 3$ are identified in the spectra of two quasars. The two most distant absorbers are at $z = 4.8668$ and 4.8823, respectively. These are the highest redshift Mg II absorbers known to date. We calculate the comoving line-of-sight number densities for the five identified Mg II absorbers. By comparing with low-redshift studies we find that the densities (dN/dz) of Mg II absorbers with $W_0^{\lambda2796} > 1.5$ Å are consistent with no cosmic evolution up to $z > 4$. We note that our sample is small. A larger sample is needed to provide a good constraint on the density evolution of Mg II absorbers.

<div align="center">REFERENCES</div>

Abazajian, K., et al. 2004, AJ, 128, 502

Baldwin, J., Ferland, G., Korista, K., & Verner, D. 1995, ApJ, 455, L119

Baldwin, J. A., Hamann, F., Korista, K. T., Ferland, G. J., Dietrich, M., & Warner, C. 2003, ApJ, 583, 649

Baldwin, J. A., Ferland, G. J., Korista, K. T., Hamann, F., & LaCluyzé, A. 2004, ApJ, 615, 610

Barth, A. J., Martini, P., Nelson, C. H., & Ho, L. C. 2003, ApJ, 594, L95

Becker, R. H., White, R. L., & Helfand, D. J. 1995, ApJ, 450, 559

Bechtold, J., et al. 2003, ApJ, 588, 119

Bertoldi, F., et al. 2003, A&A, 406, L55

Bertoldi, F., et al. 2003, A&A, 409, L47

Carilli, C. L., Bertoldi, F., Omont, A., Cox, P., McMahon, R. G., & Isaak, K. G. 2001, AJ, 122, 1679

Charlton, J. C., & Churchill, C. W. 1998, ApJ, 499, 181

Churchill, C. W., Kacprzak, G. G., & Steidel, C. C. 2005, Proceedings IAU Colloquium No. 199, Probing Galaxies through Quasar Absorption Lines, P. R. Williams, C. Shu, and B. Ménard, eds., astro-ph/0504392

Churchill, C. W., Mellon, R. R., Charlton, J. C., Jannuzi, B. T., Kirhakos, S., Steidel, C. C., & Schneider, D. P. 2000, ApJ, 543, 577

Cool, R. J., et al. 2006, AJ, 132, 823

Croton, D. J., et al. 2006, MNRAS, 365, 11

Dietrich, M., Appenzeller, I., Vestergaard, M., & Wagner, S. J. 2002, ApJ, 564, 581

Dietrich, M., Appenzeller, I., Hamann, F., Heidt, J., Jäger, K., Vestergaard, M., & Wagner, S. J. 2003, A&A, 398, 891

Dietrich, M., Hamann, F., Appenzeller, I., & Vestergaard, M. 2003, ApJ, 596, 817

Dietrich, M., & Hamann, F. 2004, ApJ, 611, 761

Djorgovski, S. G., Castro, S., Stern, D., & Mahabal, A. A. 2001, ApJ, 560, L5

Elston, R., Bechtold, J., Hill, G. J., & Ge, J. 1996, ApJ, 456, L13

Elvis, M., et al. 1994, ApJS, 95, 1

Fan, X., et al. 2000, AJ, 120, 1167

Fan, X., et al. 2001, AJ, 122, 2833

Fan, X., et al. 2003, AJ, 125, 1649

Fan, X., et al. 2004, AJ, 128, 515

Fan, X., et al. 2006, AJ, 131, 1203

Fechner, C., Baade, R., & Reimers, D. 2004, A&A, 418, 857

Foltz, C. B., Weymann, R. J., Morris, S. L., & Turnshek, D. A. 1987, ApJ, 317, 450

Freudling, W., Corbin, M. R., & Korista, K. T. 2003, ApJ, 587, L67

Friaca, A. C. S., & Terlevich, R. J. 1998, MNRAS, 298, 399

Goodrich, R. W., et al. 2001, ApJ, 561, L23

Greggio, L., & Renzini, A. 1983, A&A, 118, 217

Hamann, F., & Ferland, G. 1992, ApJ, 391, L53

Hamann, F., & Ferland, G. 1993, ApJ, 418, 11

Hamann, F., & Ferland, G. 1999, ARA&A, 37, 487

Hamann, F., Korista, K. T., Ferland, G. J., Warner, C., & Baldwin, J. 2002, ApJ, 564, 592

Hamann, F., Warner, C., Dietrich, M., & Ferland, G. 2007, in ASP Conference Proceedings, the Central Engine of Active Galactic Nuclei, ed. L. C. Ho and J.-M. Wang (San Francisco: ASP), in press (astro-ph/0701503)

Heger, A., & Woosley, S. E. 2002, ApJ, 567, 532

Hopkins, P. F., Hernquist, L., Cox, T. J., Di Matteo, T., Martini, P., Robertson, B., & Springel, V. 2005, ApJ, 630, 705

Hopkins, P. F., Hernquist, L., Cox, T. J., Di Matteo, T., Robertson, B., & Springel, V. 2006, ApJS, 163, 1

Iwamuro, F., Motohara, K., Maihara, T., Kimura, M., Yoshii, Y., & Doi, M. 2002, ApJ, 565, 63

Iwamuro, F., Kimura, M., Eto, S., Maihara, T., Motohara, K., Yoshii, Y., & Doi, M. 2004, ApJ, 614, 69

Jiang, L., et al. 2006, AJ, 132, 2127

Kauffmann, G., & Haehnelt, M. 2000, MNRAS, 311, 576

Kollmeier, J. A., et al. 2006, ApJ, 648, 128

Kurk, J. D. et al. 2007, ApJ, submitted

Li, Y., et al. 2007, ApJ, in press (astro-ph/0608190)

Lodato, G., & Natarajan, P. 2007, MNRAS, 377, L64

Madau, P., & Rees, M. J. 2001, ApJ, 551, L27

Maiolino, R., Juarez, Y., Mujica, R., Nagar, N. M., & Oliva, E. 2003, ApJ, 596, L155

Matteucci, F., & Recchi, S. 2001, ApJ, 558, 351

McGreer, I. D., Becker, R. H., Helfand, D. J., & White, R. L. 2006, ApJ, 652, 157

McIntosh, D. H., Rix, H. W., Rieke, M. J., & Foltz, C. B. 1999, ApJ, 517, L73

McLure, R. J., & Dunlop, J. S. 2004, MNRAS, 352, 1390

Nagao, T., Marconi, A., & Maiolino, R. 2006, A&A, 447, 157

Nestor, D. B., Turnshek, D. A., & Rao, S. M. 2005, ApJ, 628, 637

Pentericci, L., et al. 2002, AJ, 123, 2151

Pentericci, L., et al. 2003, A&A, 410, 75

Petric, A. O., et al. 2003, AJ, 126, 15

Priddey, R. S., Isaak, K. G., McMahon, R. G., Robson, E. I., & Pearson, C. P. 2003, MNRAS, 344, L74

Prochter, G. E., Prochaska, J. X., & Burles, S. M. 2006, ApJ, 639, 766

Rees, M. J., & Volonteri, M. 2006, Proceedings IAU Symposium No. 238, Black Holes: from Stars to Galaxies – across the Range of Masses, V. Karas and G. Matt, eds., astro-ph/0701512

Richards, G. T., et al. 2002, AJ, 124, 1

Robson, I., Priddey, R. S., Isaak, K. G., & McMahon, R. G. 2004, MNRAS, 351, L29

Shemmer, O., et al. 2006, ApJ, 644, 86

Shen, Y., et al. 2007, AJ, 133, 2222

Spergel, D. N., et al. 2007, ApJS, 170, 377

Steidel, C. C., Kollmeier, J. A., Shapley, A. E., Churchill, C. W., Dickinson, M., & Pettini, M. 2002, ApJ, 570, 526

Steidel, C. C., & Sargent, W. L. W. 1992, ApJS, 80, 1

Stern, D., et al. 2003, ApJ, 596, L39

Stoughton, C., et al. 2002, AJ, 123, 485

Trump, J. R., et al. 2006, ApJS, 165, 1

Vanden Berk, D. E., et al. 2001, AJ, 122, 549

Venkatesan, A., Schneider, R., & Ferrara, A. 2004, MNRAS, 349, L43

Vestergaard, M. & Wilkes, B. J. 2001, ApJS, 134, 1

Vestergaard, M. 2004, ApJ, 601, 676

Vestergaard, M., & Peterson, B. M. 2006, ApJ, 641, 689

Vilkoviskij, E. Y., & Irwin, M. J. 2001, MNRAS, 321, 4

Volonteri, M., & Rees, M. J. 2006, ApJ, 650, 669

Walter, F., et al. 2003, Nature, 424, 406

Walter, F., et al. 2004, ApJ, 615, L17

Wandel, A., Peterson, B. M., & Malkan, M. A. 1999, ApJ, 526, 579

Wang, R., et al. AJ, in press (astro-ph/0704.2053)

Wyithe, J. S. B., & Loeb, A. 2003, ApJ, 595, 614
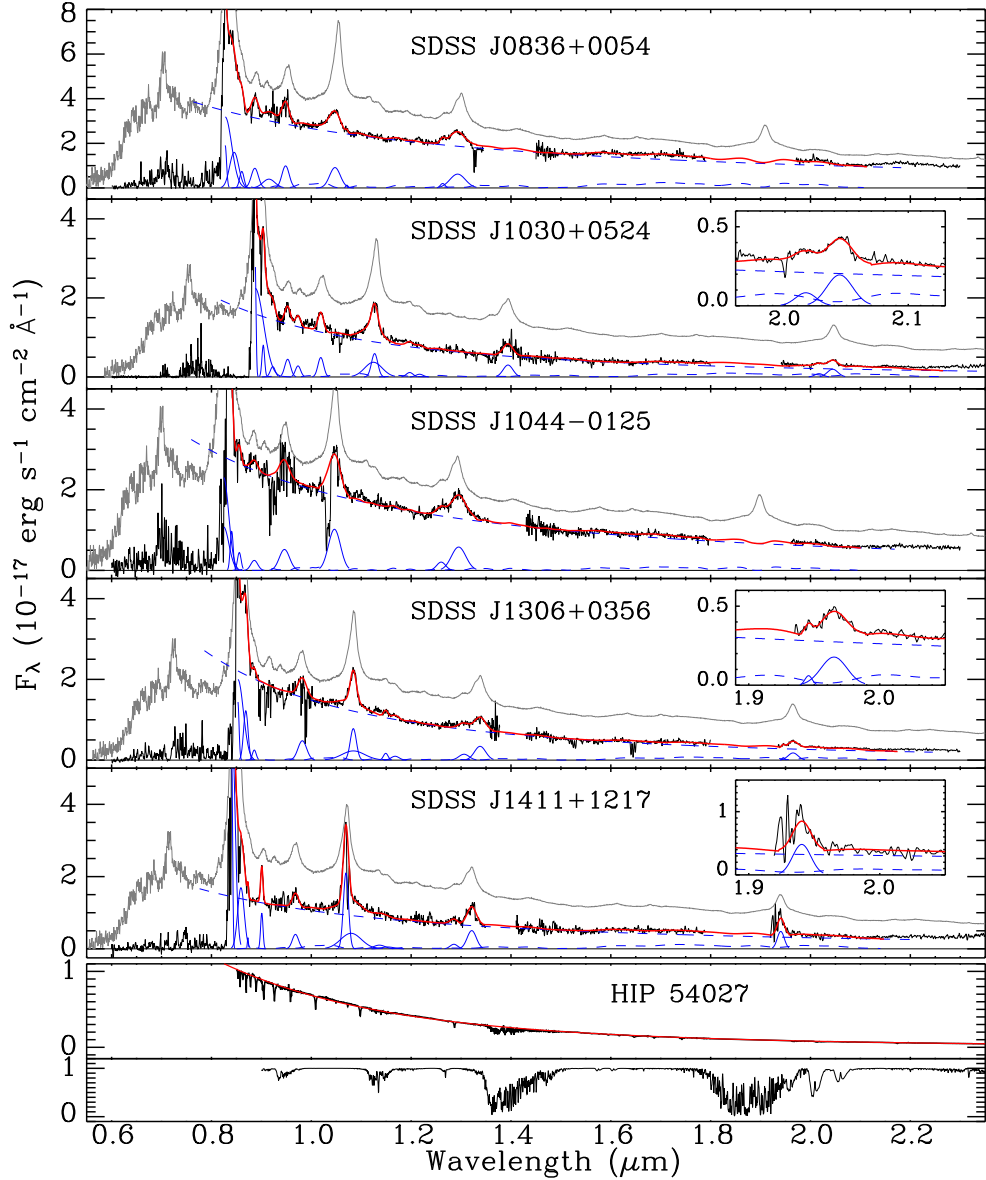
York, D. G., et al. 2000, AJ, 120, 1579

Fig. 1.— Optical and NIR spectra of five $z \sim 6$ quasars in our sample. The spectra at $\lambda > 1.0$ μm were obtained with Gemini-South/GNIRS and the spectra at $\lambda < 1.0$ μm are taken from the quasar discovery papers. The spectra have been smoothed by three pixels. The blue solid lines are the best fits to emission lines and the blue dashed lines are the best fits to the power-law continuum and Fe II emission. The red lines are the sums of all the components. For comparison, we show the low-redshift composite spectrum of Vanden Berk et al. (2001) in gray. A spectrum of a standard star HIP 54027 is also shown in the figure with a black body (with the effective temperature of HIP 54027) spectrum (in red) on top of it. The bottom panel shows the sky transparency at an airmass of 1.0 and water vapor of 1.6 mm.
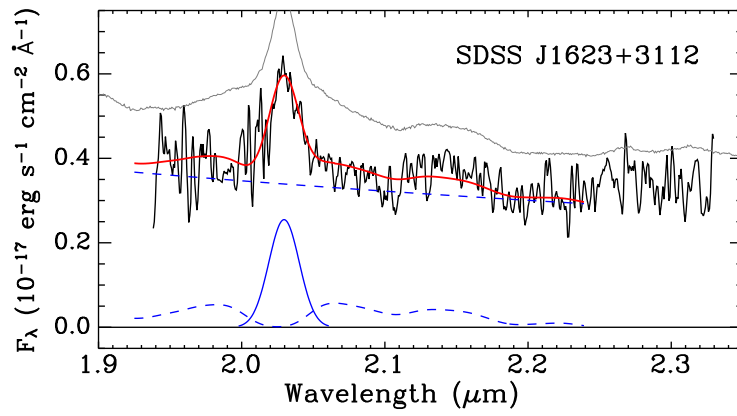
Fig. 2.— Same as Fig. 1 for SDSS J1623+3112, which was observed in K band using Gemini-North/NIRI.

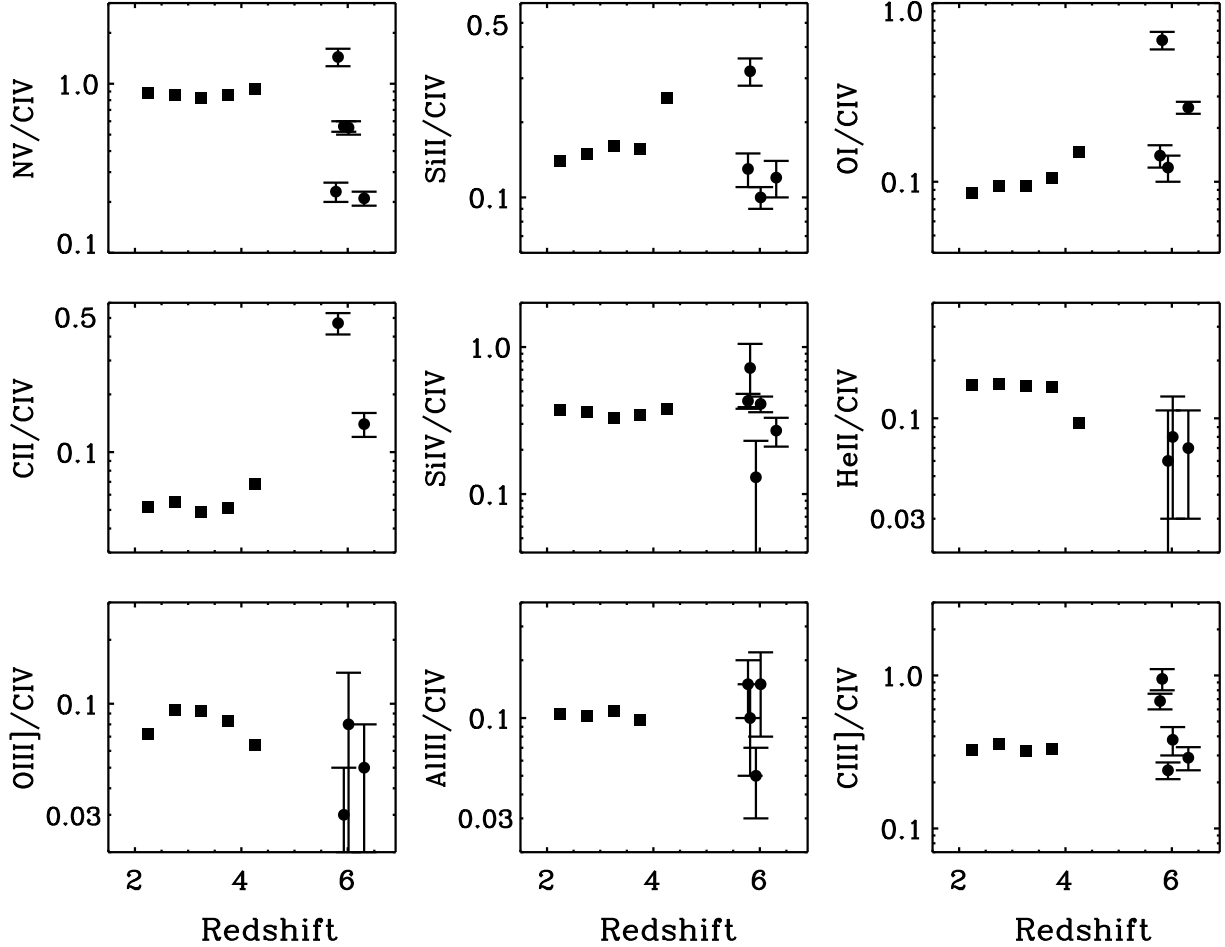Fig. 3.— Emission line fluxes (filled circles with errors) of the $z \sim 6$ quasars compared to low-redshift measurements. The fluxes have been normalized to the C IV fluxes. The filled squares represent the flux ratios measured in the composite spectra of quasars in the luminosity range $-27.5 < M_B < -26.5$ from Nagao et al. (2006). Most of the flux ratios do not exhibit strong evolution up to $z \sim 6$.
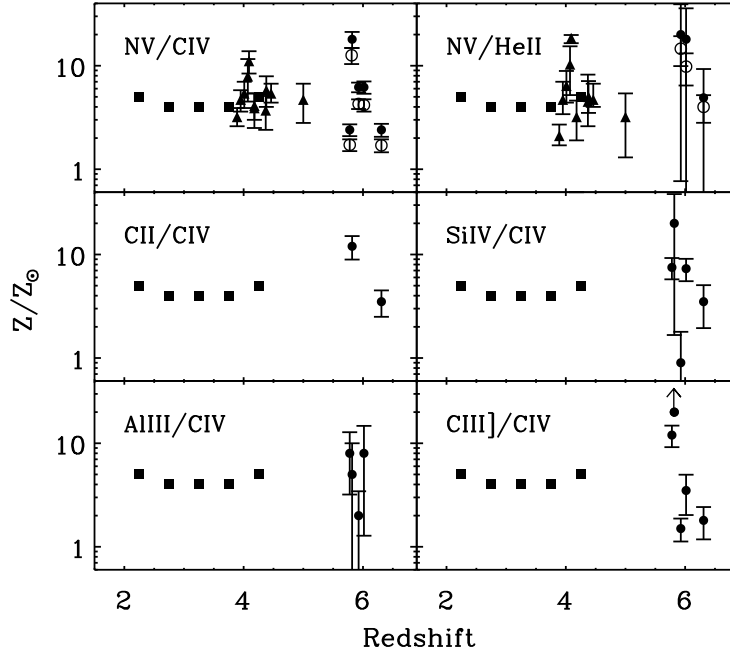
Fig. 4.— Chemical abundances of quasars derived from line ratios as a function of redshift. The open circles represent the metallicities derived from the N V/C IV and N V/He II ratios using Figure 5 of Hamann et al. (2002). The filled circles represent the metallicities derived from the line ratios using Figure 29 of Nagao et al. (2006). The filled squares show the averaged metallicities of quasars for the luminosity range $-28.5 < M_B < -25.5$ from Nagao et al. (2006). The filled triangles show the metallicities of eleven $3.9 < z < 5.0$ quasars from Dietrich et al. (2003a). The metallicities estimated from each line ratio show no strong evolution up to $z > 6$ within the errors.
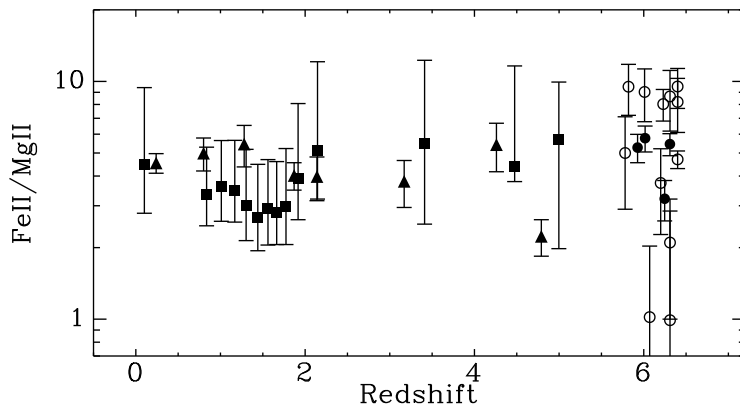
Fig. 5.— The Fe II/Mg II ratio as a function of redshift. The filled circles are our results. The open circles show the Fe II/Mg II ratios of $z \sim 6$ quasars from previous measurements (Barth et al. 2003; Maiolino et al. 2003; Freudling et al. 2003; Iwamuro et al. 2004). The filled squares and triangles represent the low-redshift results from Iwamuro et al. (2002) and Dietrich et al. (2003b). The lack of strong evolution of the Fe II/Mg II abundance continues to $z \sim 6$.

Fig. 6.— Normalized spectra of the five absorption systems in the spectra of SDSS J0836+0054 and SDSS J1306+0356. The positions of the identified lines are marked as vertical lines, and the names of the lines are given nearby. Doublets are expressed as '–D'. The four absorption systems in the spectra SDSS J1306+0356 are denoted as (a), (b), (c), and (d).
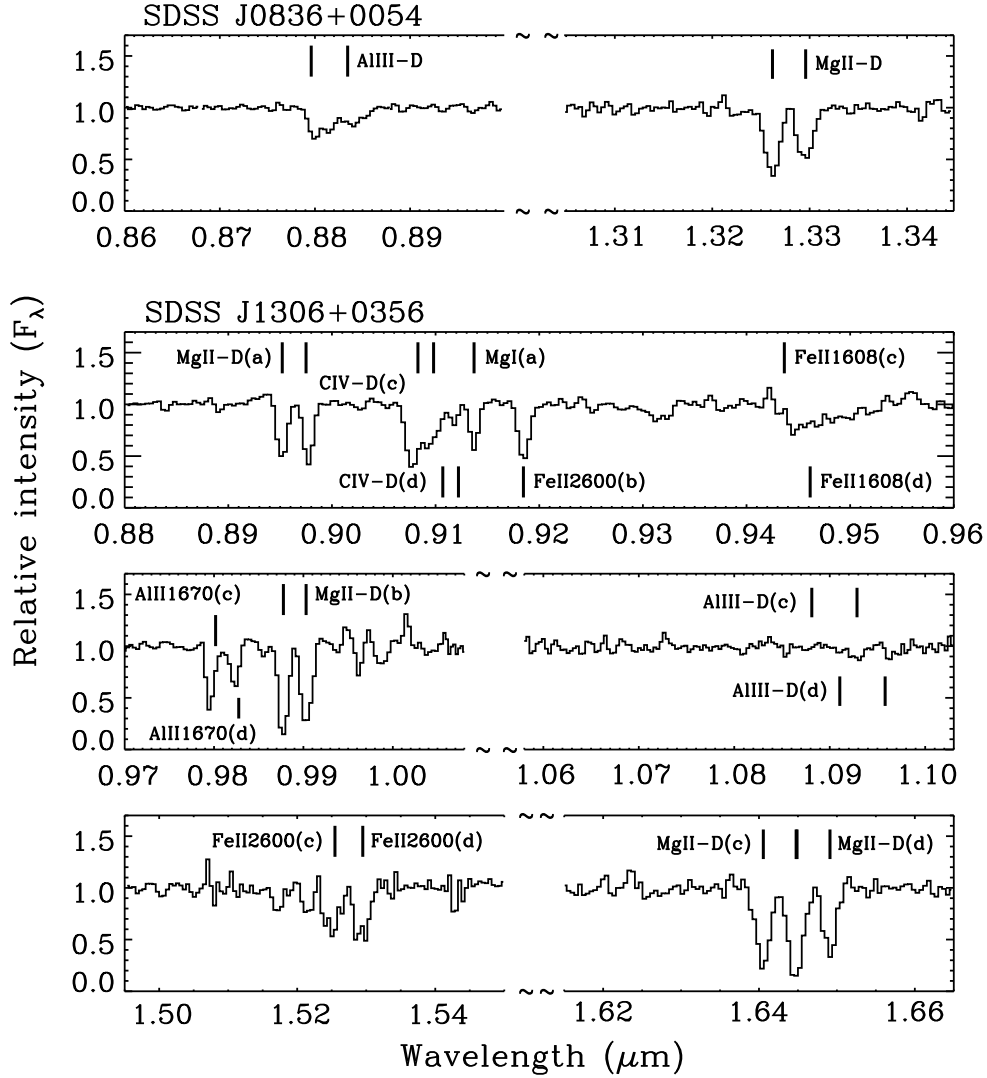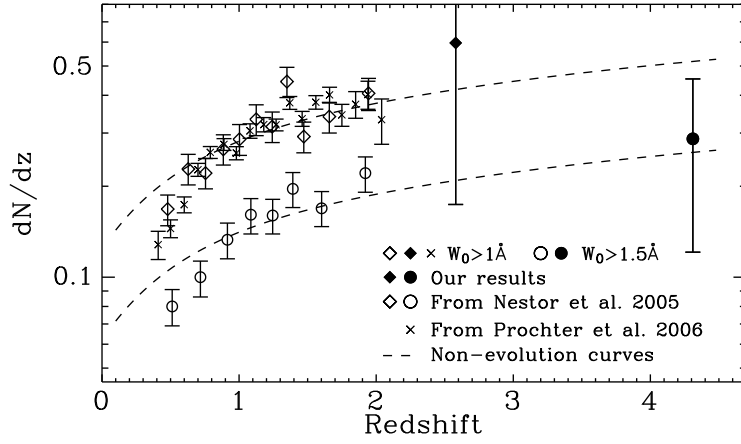
Fig. 7.— Comoving number densities of Mg II absorbers. The filled diamond represents the density for $W_0^{\lambda2796} > 1$ Å at $z = 2.6$ and the filled circle represents the density for $W_0^{\lambda2796} > 1.5$ Å at $z = 4.3$. The open diamonds and circles show the number densities for $W_0^{\lambda2796} > 1.0$ and 1.5 Å from Figure 9 of Nestor et al. (2005). The crosses show the densities of the $W_0^{\lambda2796} > 1.0$ Å absorbers from Prochter et al. (2006). The dashed lines represent non-evolution curves for the cosmology of $(\Omega_m, \Omega_\Lambda, h) = (0.3, 0.7, 0.7)$. The curves have been scaled to minimize the χ^2 to the data of Nestor et al. (2005). The densities are consistent with no cosmic evolution.

Table 1.   Log of Observations

Quasar (SDSS)	Redshift	z_{AB} (mag)	J (mag)	Date	Instrument	t_{exp} (min)
J083643.85+005453.3	5.82	18.74±0.05	17.89±0.05	2006 Feb 19	GNIRS	70
J103027.10+052455.0	6.28	20.05±0.10	18.87±0.10	2006 Mar 20, 26	GNIRS	140
J104433.04−012502.2	5.80	19.23±0.07	18.31±0.10	2006 Mar 28	GNIRS	120
J130608.26+035626.3	5.99	19.47±0.05	18.77±0.10	2006 Mar 26, 27	GNIRS	140
J141111.29+121737.4	5.93	19.65±0.08	18.95±0.05	2006 Mar 28	GNIRS	120
J162331.81+311200.5	6.22	20.09±0.10	19.15±0.10	2004 Aug 16, Sep 14	NIRI (K)	180
				2005 Aug 22, 24		

Note. — Redshifts, z_{AB} (AB magnitudes) and J (Vega-based magnitudes) are from the quasar discovery papers Fan et al. (2000), Fan et al. (2001), and Fan et al. (2004).

Table 2.   Redshifts and Continuum Slopes

Quasar (SDSS)	Redshift	$\mathrm{Slope_{uv}}(\alpha_\nu)$[a]	$\mathrm{Slope_{opt}}(\alpha_\nu)$[b]
J0836+0054	5.810 ± 0.003[c]	$-0.62^{+0.06}_{-0.06}$	-0.52
J1030+0524	6.309 ± 0.009	$0.46^{+0.18}_{-0.25}$	-0.31
J1044−0125	5.778 ± 0.005[d]	$-0.27^{+0.09}_{-0.10}$	-0.30
J1306+0356	6.016 ± 0.005	$0.50^{+0.12}_{-0.14}$	-0.12
J1411+1217	5.927 ± 0.004	$-0.21^{+0.16}_{-0.19}$	-0.51
J1623+3112	6.247 ± 0.005	$\ldots$	-0.32

[a]UV continuum slopes measured from the Gemini spectra.

[b]Optical continuum slopes taken from Jiang et al. (2006).

[c]Taken from Kurk et al. (2007).

[d]Measured from the C III] $\lambda1909$ emission line.

Table 3.   Emission Line Properties

		J0836+0054	J1030+0524	J1044−0125	J1306+0356	J1411+1217	J1623+3112
N v	EW	15.9±0.7	4.9±0.1	3.9±0.2	9.3±0.3	28.9±0.4	. . .
	FWHM	31.5±1.0	8.7±0.2	10.4±0.3	15.0±0.2	22.3±0.3	. . .
Si ii	EW	3.6±0.3	3.0±0.2	2.3±0.1	1.7±0.1	0.9±0.1	. . .
	FWHM	15.0±0.6	15.8±0.7	12.7±0.3	12.8±0.4	3.7±0.3	. . .
O i	EW	7.4±0.1	6.7±0.3	2.6±0.2	. . .	6.7±0.2	. . .
	FWHM	24.6±0.5	18.8±0.7	24.3±1.3	. . .	8.1±0.2	. . .
C ii	EW	5.8±0.5	4.0±0.4	. . .	. . .	. . .	. . .
	FWHM	41.9±3.1	17.0±1.5	. . .	. . .	. . .	. . .
Si iv	EW	9.3±4.2	8.5±1.7	8.9±0.7	9.5±0.8	8.1±6.4	. . .
	FWHM	25.3±5.9	18.4±2.9	35.7±1.8	29.0±2.0	21.5±12.2	. . .
C iv	EW	15.0±1.6	40.0±3.1	24.7±2.1	29.6±2.4	76.2±5.8	. . .
	FWHM	37.1±3.0	27.3±2.9	42.2±3.1	24.5±2.3	17.5±1.6	. . .
He ii	EW	. . .	3.4±2.0	. . .	2.6±1.8	5.1±2.5	. . .
	FWHM	. . .	21.7±8.8	. . .	15.5±7.5	39.0±26.8	. . .
O iii]	EW	. . .	2.3±1.3	. . .	2.7±2.0	2.8±2.5	. . .
	FWHM	. . .	22.9±11.0	. . .	26.9±19.4	42.2±34.0	. . .
Al iii	EW	1.8±0.9	. . .	5.0±1.6	7.0±3.1	5.1±2.3	. . .
	FWHM	16.3±6.8	. . .	31.0±6.7	34.5±14.7	25.6±9.2	. . .
C iii]	EW	18.9±2.3	19.3±2.8	24.0±1.8	19.1±3.9	26.1±3.2	. . .
	FWHM	53.2±4.9	31.6±3.3	50.3±3.2	37.6±7.4	31.3±2.6	. . .
Mg ii	EW	. . .	46.1±3.7	. . .	24.9±2.1	37.5±5.5	27.4±3.9
	FWHM	. . .	33.8±2.2	. . .	33.2±2.2	23.7±2.7	34.4±2.4

Note. — Rest-frame FWHM and EW are in units of Å.

Table 4.   Flux Ratios

	J0836+0054	J1030+0524	J1044−0125	J1306+0356	J1411+1217	J1623+3112
N v/C iv	1.44±0.17	0.21±0.02	0.23±0.03	0.55±0.05	0.56±0.04	. . .
Si ii/C iv	0.32±0.04	0.12±0.02	0.13±0.02	0.10±0.01	0.02±0.01	. . .
O i/C iv	0.62±0.07	0.26±0.02	0.14±0.02	. . .	0.12±0.02	. . .
C ii/C iv	0.47±0.06	0.14±0.02	. . .	. . .	. . .	. . .
Si iv/C iv	0.72±0.33	0.27±0.06	0.43±0.05	0.41±0.05	0.13±0.10	. . .
He ii/C iv	. . .	0.07±0.04	. . .	0.08±0.05	0.06±0.05	. . .
O iii]/C iv	. . .	0.05±0.03	. . .	0.08±0.06	0.03±0.02	. . .
Al iii/C iv	0.10±0.05	. . .	0.15±0.05	0.15±0.07	0.05±0.02	. . .
C iii]/C iv	0.95±0.15	0.29±0.05	0.68±0.08	0.38±0.08	0.24±0.03	. . .
Fe ii/Mg ii	. . .	5.45±0.58	. . .	5.77±0.72	5.27±0.72	3.21±0.62

Table 5.   Central BH Masses (10^9 M$_\odot$)

Quasar (SDSS)	L_{Bol}[a]	L_{Bol}/L_{Edd}[b]	$M_{BH}(C\,IV)$	$M_{BH}(Mg\,II)$	$M'_{BH}(Mg\,II)$[c]
J0836+0054	47.72	0.44	9.3±1.6	. . .	. . .
J1030+0524	47.37	0.50	3.6±0.9	1.0±0.2	2.1±0.4
J1044−0125	47.63	0.31	10.5±1.6	. . .	. . .
J1306+0356	47.40	0.61	3.2±0.6	1.1±0.1	2.2±0.3
J1411+1217	47.20	0.94	1.3±0.3	0.6±0.1	0.9±0.2
J1623+3112	47.33	1.11	. . .	1.5±0.3	. . .

[a]Bolometric luminosity in log[erg s^{-1}] from Jiang et al. (2006).

[b]L_{Edd} is derived from $M_{BH}(C\,IV)$ except for SDSS J1623+3112, whose L_{Edd} is derived from $M_{BH}(Mg\,II)$.

[c]M'_{BH} is estimated from the new relation by Vestergaard et al. (in preparation).

Table 6.   Absorption Lines

Absorption system	λ_{abs} (Å)	ID	z_{abs}	W_0 (Å)
SDSS J0836+0054	13261.81	Mg II(2796)	3.7426	2.59
	13295.43	Mg II(2803)	3.7424	2.08
SDSS J1306+0356 (a)	8952.03	Mg II(2796)	2.2013	1.86
	8977.30	Mg II(2803)	2.2022	1.99
	9137.13	Mg I(2852)	2.2028	1.29
SDSS J1306+0356 (b)	9877.64	Mg II(2796)	2.5323	3.24
	9903.27	Mg II(2803)	2.5324	3.15
	9185.23	Fe II(2600)	2.5325	1.94
SDSS J1306+0356 (c)	16405.55	Mg II(2796)	4.8668	2.92
	16447.67	Mg II(2803)	. . .	. . .
	9795.84	Al II(1670)	4.8632	1.11
	15252.21	Fe II(2600)	4.8658	1.49
SDSS J1306+0356 (d)	16448.85	Mg II(2796)	. . .	. . .
	16491.08	Mg II(2803)	4.8823	2.11
	9822.93	Al II(1670)	4.8795	0.76
	15293.94	Fe II(2600)	4.8819	1.97